

# Simulation of Energetic Neutral Atom Images at Venus

H. Gunell\* and M. Holmström

*Swedish Institute of Space Physics, Kiruna, Sweden*

H. K Biernat, H. Lammer, H. Lichtenegger, and T. Penz  
*Space Research Institute, Austrian Academy of Sciences, Graz, Austria*

N. V. Erkaev

*Institute of Computational Modelling, Russian Academy of Sciences, Russia*

We present simulated images of energetic neutral atoms (ENAs) produced in charge exchange collisions between solar wind protons and neutral atoms in the exosphere of Venus, and make a comparison with earlier results for Mars. The images are found to be dominated by two local maxima. One produced by charge exchange collisions in the solar wind, upstream of the bow shock, and the other close to the dayside ionopause. The simulated ENA fluxes at Venus are lower than those obtained in similar simulations of ENA images at Mars at solar minimum conditions, and close to the fluxes at Mars at solar maximum. Our numerical study shows that the ENA flux decreases with an increasing ionopause altitude. The influence of the Venus nighttime hydrogen bulge on the ENA emission is small.

## I. INTRODUCTION

Energetic neutral atoms (ENAs) are produced in charge exchange collisions between solar wind protons and neutral atoms in the upper part of the atmospheres of the planets. ENA images of Earth's magnetosphere have been obtained by instruments on the IMAGE satellite [1]. Holmström, et al., [2] simulated images of ENAs produced by the interaction between the solar wind and Mars through the integration of the ENA production along lines of sight to a virtual ENA instrument.

In this work ENA images of the region where the solar wind interacts with Venus' atmosphere are calculated. To simulate an ENA image one needs a model for how the density of the neutral gas species varies as a function of the spatial coordinates, a model for the plasma density and temperature, and knowledge of the cross sections for charge exchange collisions between protons and the neutral gas.

Due to the scarcity of in situ measurements the ionopause altitude at Venus is not well known [3]. It is thought to vary with the solar cycle, but since all in situ measurements were made during solar maximum conditions this variation is still unconfirmed. We investigate the ENA emissions as a function of ionopause distance by scaling the ionopause altitude in the plasma model through the range from 250 km to 500 km. The ionopause is thought to be close to the lower end of that range at solar minimum because of the lower ionospheric pressure [3].

The plasma model used in this work is a semi-analytical MHD model [4–6]. It is semi-analytical in that it numerically finds steady state solutions to the MHD equations, assuming analytical expressions for the shape of the ionopause and bow shock, and for the spatial variation of the total pressure. The input parameters of the solar wind are shown in table I, and the boundary conditions were described by [6].

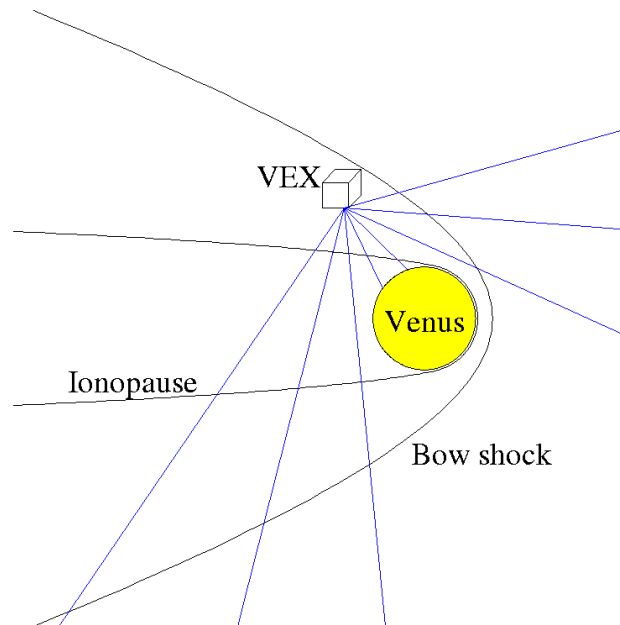
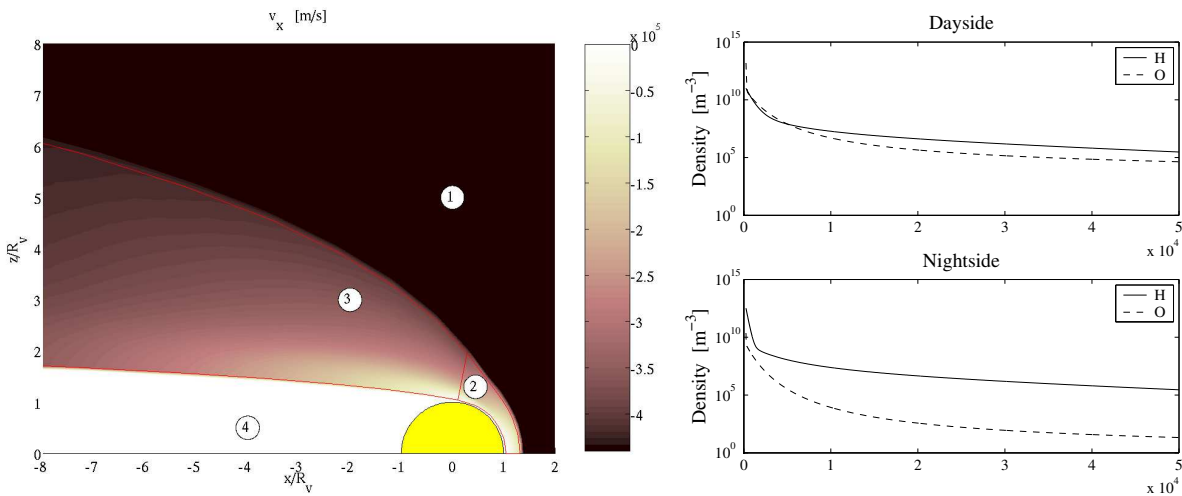
TABLE I: Solar wind parameters used in the MHD simulations of Venus in this work, and those used in ref. [7] and [2] for Mars.

	Venus	Mars (Ma et al.)	Mars Holmström et al.
Electron number density	$1.5 \times 10^7 \text{m}^{-3}$	$4 \times 10^6 \text{m}^{-3}$	$2.5 \times 10^6 \text{m}^{-3}$
Solar wind speed	$4.4 \times 10^5 \text{m/s}$	$5 \times 10^5 \text{m/s}$	$4 \times 10^5 \text{m/s}$
Solar wind temperature	$2 \times 10^5 \text{K}$	$1.75 \times 10^5 \text{K}$	$1.2 \times 10^5 \text{K}$
Solar wind magnetic field	$1.2 \times 10^{-8} \text{T}$	$3 \times 10^{-9} \text{T}$	

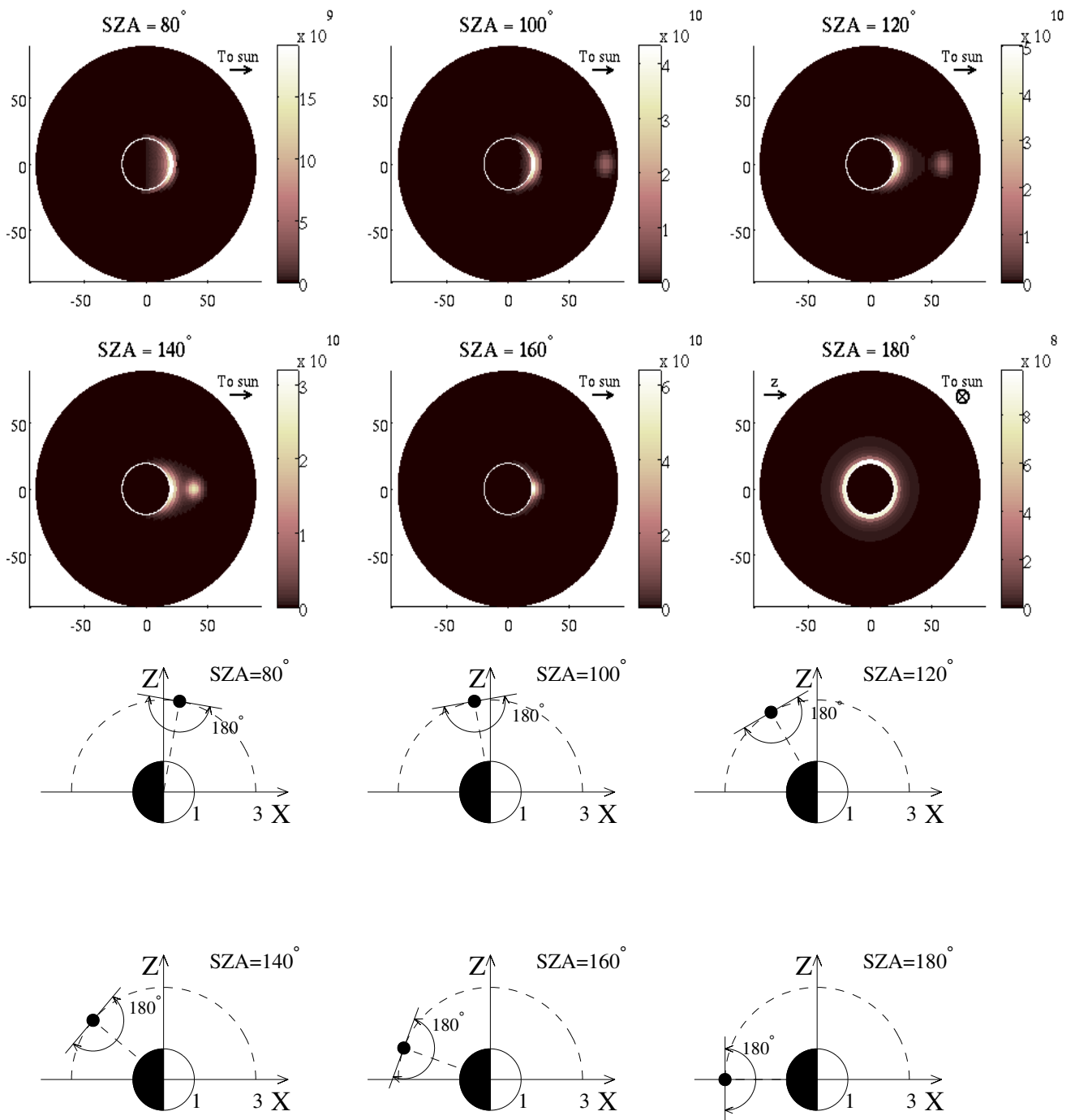
\*Electronic address: [herbert.gunell@physics.org](mailto:herbert.gunell@physics.org); URL: <http://www.irf.se/~herbert>

To generate ENA images from simulations we need:

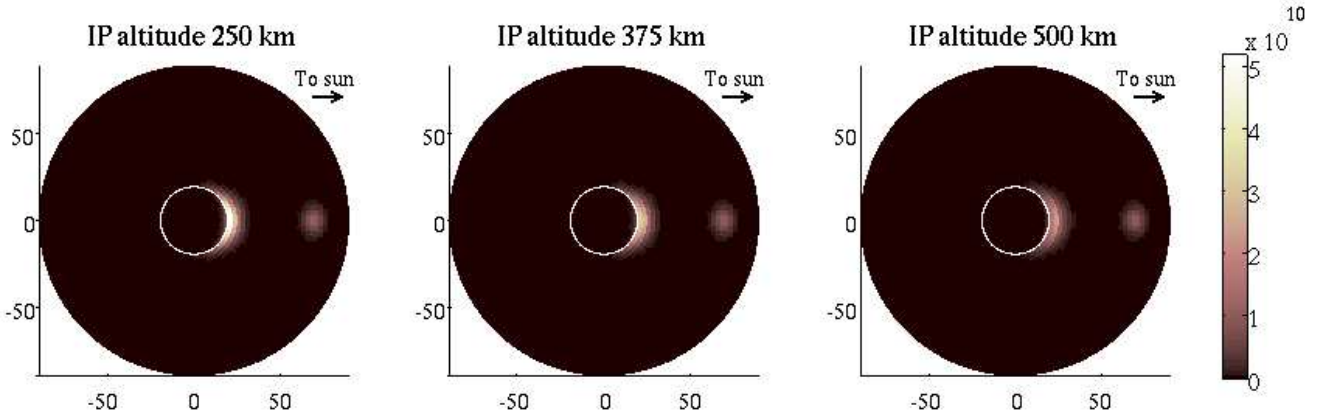
1. A model of the plasma flow around Venus. We have used a semi-analytical MHD model developed by Helfried Biernat and Nikolai Erkaev [4–6].
2. A model of the neutral gas density. Measurements of the neutral density, near the equator, have been made by the Pioneer Venus Orbiter (and other spacecraft) [8–12].



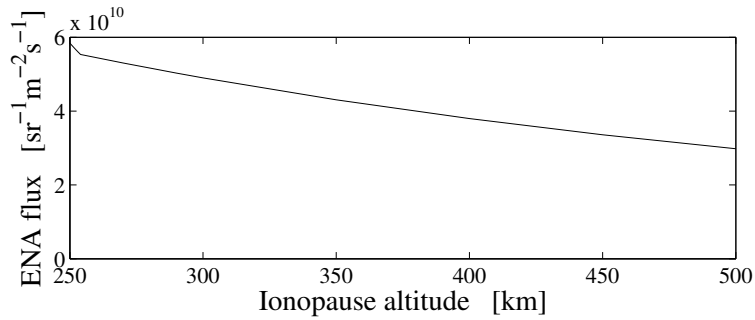
# ENA images from different solar zenith angles



# Varying the ionopause altitude



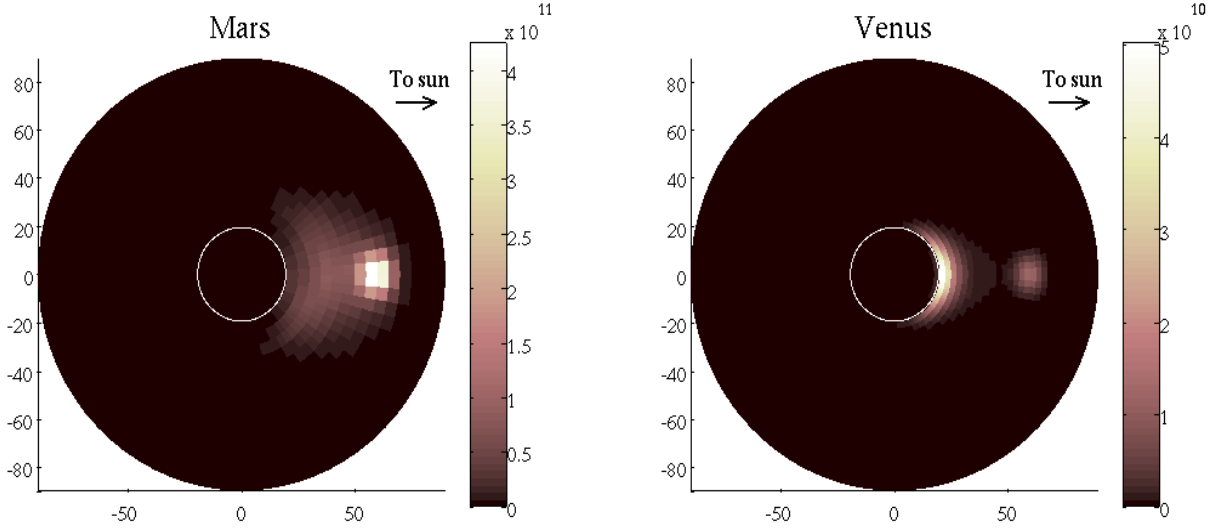
ENA images with 250 km ionopause altitude (left panel), 375 km (middle panel), and 500 km (right panel). The vantage point is in the  $xz$ -plane at  $3R_v$  planetocentric distance with a solar zenith angle of  $110^\circ$  for all three images. The ENA flux decreases with an increasing ionopause altitude, i.e. going from the left to the right panel. The maximum also moves slightly away from the planet with the increasing ionopause altitude.



Maximum flux, as observed by a virtual instrument in the  $xz$ -plane  $3R_v$  from the centre of Venus, shown as a function of the subsolar ionopause altitude. The decrease of the maximum ENA flux with ionopause altitude is a result of the decrease in neutral gas density with altitude.

The ENA flux from the local emission maximum near the planet decreases with increasing ionopause altitude, since with a higher ionopause altitude the protons pass through a region with lower neutral density. The maximum moves slightly outward from the planet as the ionopause altitude increases. The maximum that corresponds to ENAs produced upstream in the solar wind remains unchanged by changes in the ionopause altitude. The decrease of the maximum ENA flux with ionopause altitude is a result of the decrease in neutral gas density with altitude. As the ionopause is scaled to higher altitudes the bulk proton flow passes through regions with lower neutral gas density.

# Comparing Mars and Venus

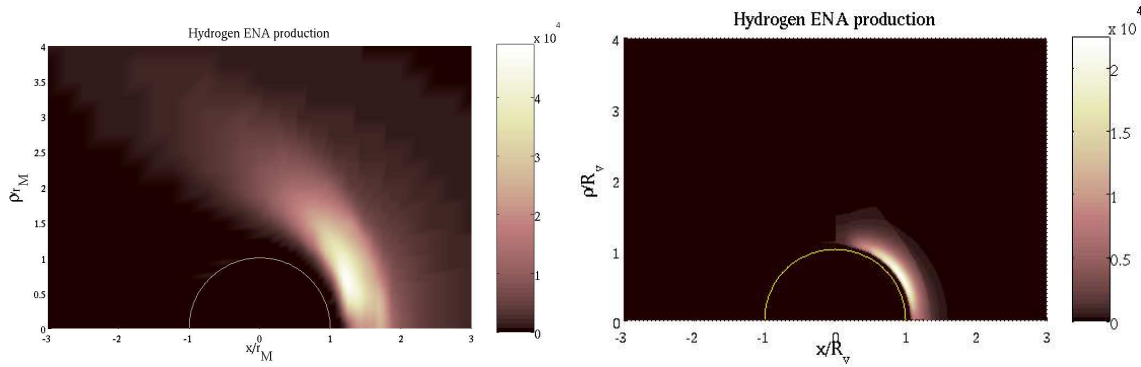


ENA images from Mars (left) and Venus (right) from vantage points with solar zenith angles of  $120^\circ$  and planetocentric distance three radii of the respective planet. The image of the Martian environment is based on an MHD model of the plasma flow around Mars [7].

TABLE II: A comparison of some aspects of the results from Venus and Mars. Values for Venus are given for ionopause altitudes 250 km and 400 km respectively. Venus' upper atmosphere is approximately the same independent of the solar cycle. The values for Mars from ref. [2] are all for solar minimum conditions. Values from the MHD simulation of Mars were taken from ref. [13]. "Max. flux" refers to the maximum flux in an ENA image of the interaction region downstream of the bow shock. Solar minimum and maximum conditions are denoted by "min" and "max" respectively.

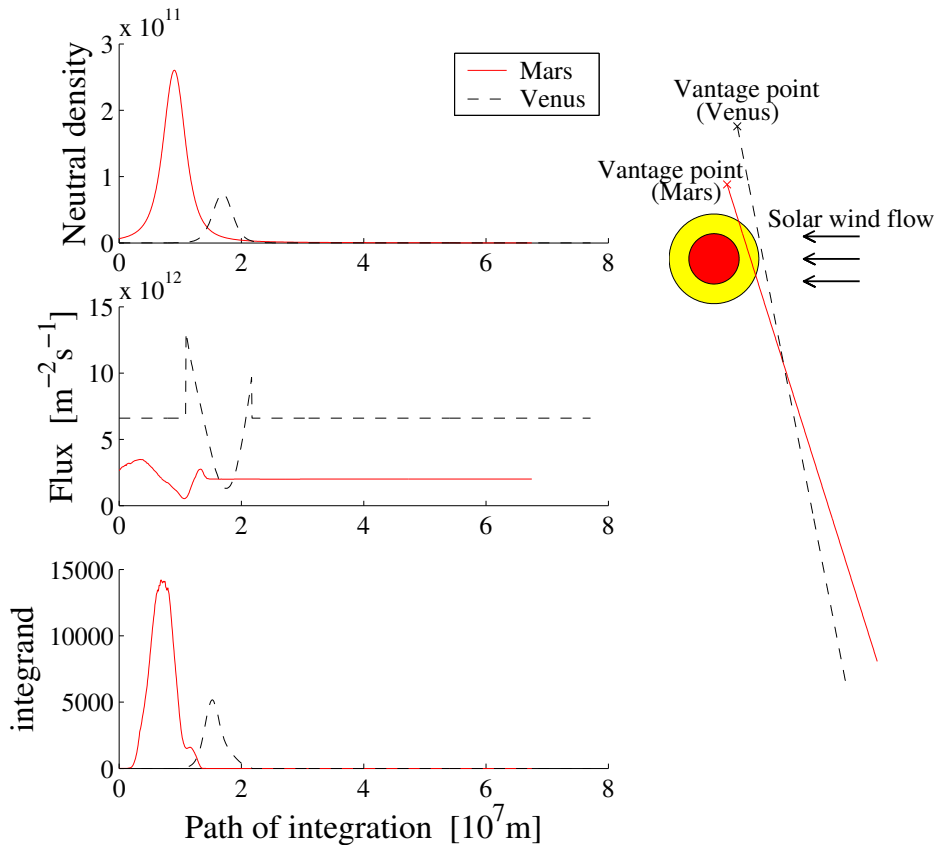
	Venus IP 250 km	Venus IP 400 km	Mars Holmström	Mars MHD	unit
Production rate	$7.8 \cdot 10^{24}$	$5.6 \cdot 10^{24}$	$1.7 \cdot 10^{25}$	$\left\{ \begin{array}{l} 2.4 \cdot 10^{25}, \text{ min} \\ 5.1 \cdot 10^{24}, \text{ max} \end{array} \right.$	$\text{s}^{-1}$
Escape rate	$5.3 \cdot 10^{24}$	$4.0 \cdot 10^{24}$	$1.5 \cdot 10^{25}$		$\text{s}^{-1}$
Precip. rate	$2.2 \cdot 10^{24}$	$1.2 \cdot 10^{24}$	$1.4 \cdot 10^{24}$		$\text{s}^{-1}$
Max. flux	$5.8 \cdot 10^{10}$	$3.8 \cdot 10^{10}$	$3 \cdot 10^{11}$	$1.1 \cdot 10^{11}, \text{ min}$	$\text{sr}^{-1}\text{m}^{-2}\text{s}^{-1}$

# Production rate maps



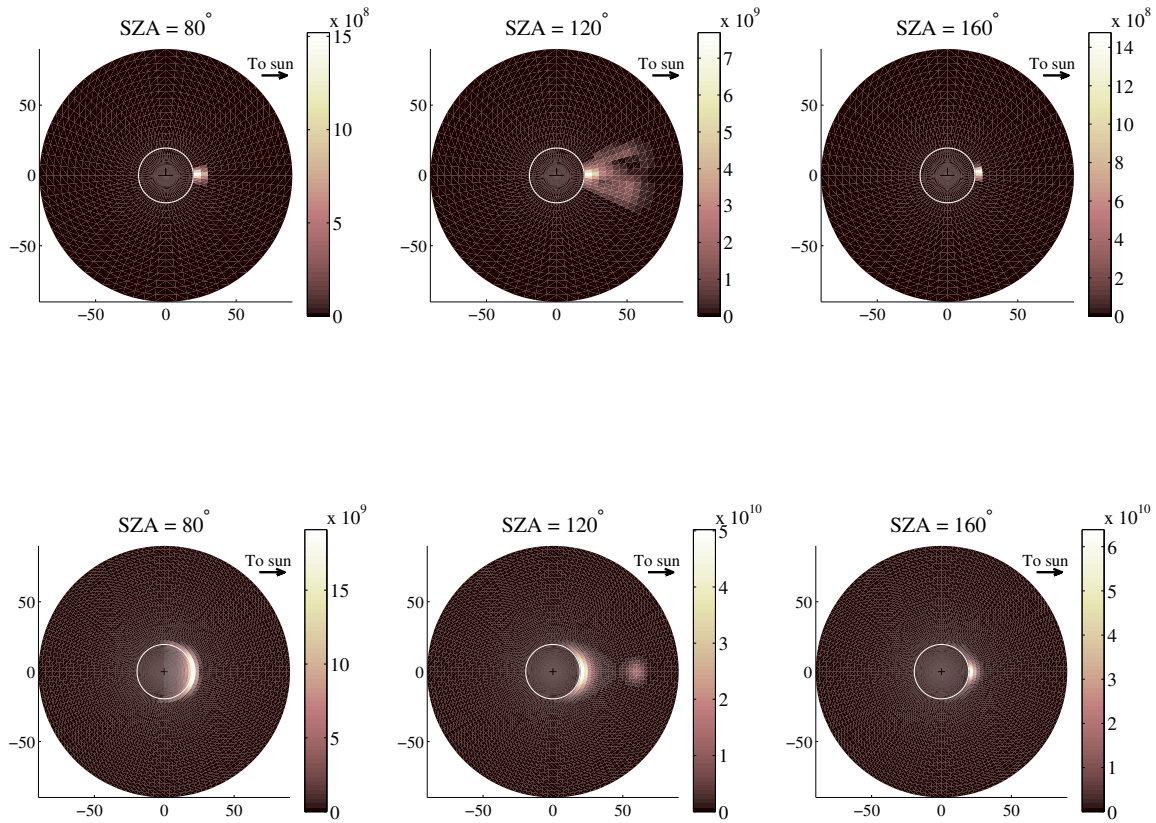
ENA production rate at Mars (left), and Venus (right), shown in a cylindrical coordinate system. The production rate is shown in units of  $\text{m}^{-3}\text{s}^{-1}$ . The total production rate for Venus is  $5.6 \times 10^{24} \text{ s}^{-1}$ . For an ionopause altitude of 250 km the total production rate is  $7.8 \times 10^{24} \text{ s}^{-1}$ . For Mars it is  $2.4 \times 10^{25} \text{ s}^{-1}$  (c.f. table II).

# Line of sight integrals



The total neutral gas density, the plasma flux, and the rate of ENA production in the direction toward the vantage point, along the line of sight from the vantage point.

# Comparing different models



ENA images calculated using the gas dynamical model by Spreiter and Stahara (top), and ENA images calculated using the MHD model by Biernat and Erkaev (bottom).

## II. CONCLUSIONS

We have simulated ENA images of the Venus-solar wind interaction region, and studied the dependence of the ENA flux on the ionopause position by scaling the plasma results of the MHD calculation. The main contribution to the ENA flux observed in the ENA images stems from a region of space between the ionopause and the bow shock on the dayside of the planet.

The maximum flux observed at  $3R_v$  planetocentric distance, coming from the interaction region on the dayside of Venus, is  $5.8 \times 10^{10} \text{ sr}^{-1}\text{m}^{-2}\text{s}^{-1}$ , which occurs for the lowest ionopause altitude, i.e. 250 km. The ENAs that are produced in the solar wind upstream of the bow shock are not included in this number. For higher ionopause altitudes the ENA flux decreases, and is below  $3.8 \times 10^{10} \text{ sr}^{-1}\text{m}^{-2}\text{s}^{-1}$ , when the subsolar ionopause is at 400 km altitude. The corresponding number for Mars at solar minimum conditions, computed by Holmström, et al., [2] is about  $3 \times 10^{11} \text{ sr}^{-1}\text{m}^{-2}\text{s}^{-1}$ , which is five times larger than the value obtained for Venus with an ionopause altitude of 250 km. The ENA production rate at Mars at solar maximum conditions is about the same as that at Venus.

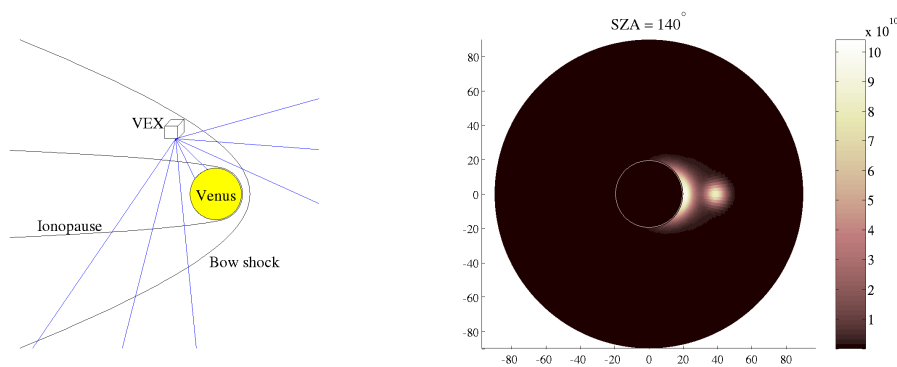
In comparison with Mars the ENA fluxes and the total ENA production rates at Venus are lower. This is explained by the neutral corona which extends further into space at Mars than at Venus. Thus the neutral gas density at Mars is higher than at Venus in the altitude range that is important for ENA production. It can also be seen in the ENA images that the ENA production is concentrated closer to the planet at Venus than at Mars.

At the present time no measured ENA images of Venus are available. Also the measurements of the components that determine the ENA flux and the morphology of the images, i.e. the neutral density and the density, temperature, and bulk velocity of the plasma, are quite scarce. Furthermore the solar wind parameters vary substantially with time. This means that there are considerable uncertainties in the input parameters of the numerical calculations of ENA images, due to the uncertainties in the solar wind parameters and in the neutral densities of the upper atmospheres. It also means that the output of a solar wind-planetary interaction model, i.e., plasma density, temperature, and bulk velocity in the vicinity of the planet, cannot be checked by comparison with measured data. An MHD model neglects all kinetic and finite gyro radius effects, which may turn out to be important for ENA imaging. Hybrid models, which treat the electrons as a fluid and the ions as particles, take kinetic and finite gyro radius effects into account, but instead suffer from worse accuracy, since limited computer resources requires the use of large grid cell size and a small number of particles. The differences between different models and the implications for ENA imaging is discussed further by [13].

It is interesting to compare the results obtained here with the results of Fok, et al., [14]. Although their parameters are not exactly the same as ours they are at least similar. Fok, et al., [14] took the effect of space craft motion into account. We do not. Since we are considering ENAs with energies above 50 eV this amounts only to a small correction in our case. We have calculated ENA images from the same vantage points that were used in Fig. 5 of ref. [14]. Both models yield ENA fluxes of the same order of magnitude. In one case the flux calculated here is larger and in the other case it is smaller than that calculated by [14]. The difference could be caused by differences in the models of the neutral density and the plasma flow, but it can also be an effect of the finite resolution of the figures and that Fok, et al., include ENAs with energies down to 2 eV, whereas our lower energy limit is 50 eV. We conclude that the two models are in reasonable agreement considering the uncertainties of the models. Real measurements will be required to determine between them, or indeed to say anything conclusively about the accuracy of the models.

## Summary and conclusions

- We have presented simulated ENA images of the interaction between the solar wind and Venus' upper atmosphere.
- These images are based on a semi-analytical MHD model of the plasma flow, that was developed by Helfried Biernat and Nikolai Erkaev.
- And on a model of the neutral gas density based on measured data that is available in the literature.
- The images are dominated by two local maxima. One produced by charge exchange collisions in the solar wind, upstream of the bow shock, and the other close to the dayside ionopause.
- The simulated ENA fluxes at Venus are lower than those obtained in similar simulations of ENA images at Mars at solar minimum, and roughly equal at solar maximum.
- The gas dynamical model by Spreiter and Stahara yields lower ENA fluxes.



- 
- [1] J. L. Burch, S. B. Mende, D. G. Mitchell, T. E. Moore, C. J. Pollock, B. W. Reinisch, B. R. Sandel, S. A. Fuselier, D. L. Gallagher, J. L. Green, J. D. Perez, and P. H. Reiff, "Views of Earth's magnetosphere with the IMAGE satellite," *Science*, vol. 291, no. 5504, pp. 619–624, 2001.
  - [2] M. Holmström, S. Barabash, and E. Kallio, "Energetic neutral atoms at Mars I: Imaging of solar wind protons," *Journal of Geophysical Research*, vol. 107, no. A10, 2002.
  - [3] J. G. Luhmann, "Comparative studies of the solar wind interaction with weakly magnetized planets," *Advances in Space Research*, vol. 12, no. 9, pp. 191–203, 1992.
  - [4] H. K. Biernat, N. V. Erkaev, and C. J. Farrugia, "Aspects of MHD flow about Venus," *Journal of Geophysical Research*, vol. 104, pp. 12617–12626, 1999.
  - [5] H. K. Biernat, N. V. Erkaev, and C. J. Farrugia, "MHD effects in the Venus magnetosheath," *Advances in Space Research*, vol. 26, pp. 1587–1591, 2000.
  - [6] H. K. Biernat, N. V. Erkaev, and C. J. Farrugia, "MHD effects in the Venus magnetosheath including mass loading," *Advances in Space Research*, vol. 28, pp. 833–839, 2001.
  - [7] Y. Ma, A. F. Nagy, K. C. Hansen, D. L. DeZeeuw, and T. I. Gombosi, "Three-dimensional multispecies MHD studies of the solar wind interaction with Mars in the presence of crustal fields," *Journal of Geophysical Research*, vol. 107, no. A10, 2002.
  - [8] H. C. Brinton, H. C. Taylor, Jr., H. B. Niemann, H. G. Mayr, A. F. Nagy, T. E. Cravens, and D. F. Strobel, "Venus nighttime hydrogen bulge," *Geophysical Research Letters*, vol. 7, pp. 865–868, 1980.
  - [9] J. M. Rodriguez, M. J. Prather, and M. B. McElroy, "Hydrogen on Venus: exospheric distribution and escape," *Planetary and Space Science*, vol. 32, pp. 1235–1255, 1984.
  - [10] J. G. Mengel, D. R. Stevens-Rayburn, H. G. Mayr, and I. Harris, "Non-linear three dimensional spectral model of the Venusian thermosphere with super-rotation—II. temperature composition and winds," *Planetary and Space Science*, vol. 37, pp. 707–722, 1989.
  - [11] M. B. McElroy, M. J. Prather, and J. M. Rodriguez, "Loss of oxygen from Venus," *Geophysical Research Letters*, vol. 9, pp. 649–651, 1982.
  - [12] A. F. Nagy, T. E. Cravens, J.-H. Yee, and A. I. F. Stewart, "Hot oxygen atoms in the upper atmosphere of Venus," *Geophysical Research Letters*, vol. 8, pp. 629–632, 1981.
  - [13] H. Gunell, M. Holmström, S. Barabash, E. Kallio, P. Janhunen, A. F. Nagy, and Y. Ma, "Planetary ENA imaging: II. effects of different interaction models for mars," submitted to *Planetary and Space Science*, 2004.
  - [14] M.-C. Fok, T. E. Moore, M. R. Collier, and T. Tanaka, "Neutral atom imaging of solar wind interaction with the Earth and Venus," *Journal of Geophysical Research*, vol. 109, no. A1, 2004.